Doping variation of anisotropic charge and orbital dynamics in $Y_{1-x}Ca_xVO_3$: Comparison with $La_{1-x}Sr_xVO_3$

J. Fujioka,[1] S. Miyasaka,[2] and Y. Tokura[1,3,4]
[1]*Department of Applied Physics, University of Tokyo, Tokyo 113-8656, Japan*
[2]*Department of Physics, University of Osaka, Osaka 560-0043, Japan*
[3]*ERATO-Multiferroics Project, Japan Science and Technology Agency, Tsukuba, 305-8562, Japan*
[4]*Cross-Correlation Materials Research Program (CMRG), RIKEN, Wako 351-0198, Japan*
(Received 24 January 2008; revised manuscript received 13 March 2008; published 2 April 2008)

The doping variation of charge and orbital dynamics in perovskite-type $Y_{1-x}Ca_xVO_3$ ($0 \leq x \leq 0.1$) is investigated by measurements of the optical conductivity and Raman scattering spectra in comparison to the larger bandwidth system $La_{1-x}Sr_xVO_3$. We also take into consideration the magnitude of the $GdFeO_3$-type orthorhombic lattice distortion, which is large and small in $Y_{1-x}Ca_xVO_3$ and $La_{1-x}Sr_xVO_3$, respectively, and discuss its effect on the evolution of charge dynamics. The optical conductivity spectra show that the doped hole is well localized and forms the small polaronlike state. The hole dynamics in $Y_{1-x}Ca_xVO_3$ is nearly isotropic up to the doping level of the orbital order-disorder transition, while that in $La_{1-x}Sr_xVO_3$ is anisotropic in the lightly doped region due to the one-dimensional orbital exchange interaction. The possible origin of the difference in the hole dynamics is discussed in terms of the local lattice distortion, which is induced by the formation of the small polaronlike state and becomes more significant for the reduced one-electron bandwidth. In addition, the optical Mott-gap excitation in the nominally *C*-type spin and *G*-type orbital ordered phase is distinct from that for $La_{1-x}Sr_xVO_3$ in its intensity and spectral shape. This suggests that the orthorhombic lattice distortion enhances the modification of the spin and orbital ordering from the pure *C* type and *G* type, respectively. The systematic study of Raman scattering spectra has shown that the dynamic *G*-type spin and *C*-type orbital correlation subsists at low temperatures in the doping induced phase of the nominally *C*-type spin ordering and *G*-type orbital ordering.

DOI: 10.1103/PhysRevB.77.144402 PACS number(s): 71.30.+h, 72.15.−v, 78.20.−e, 75.30.Et

I. INTRODUCTION

Recent investigations on the 3*d* transition-metal oxides have revealed the important interplay among charge, spin, and orbital degrees of freedom in the dramatic change of the electronic and magnetic structures, such as superconductivity, colossal magnetoresistance, metal-insulator transition, and charge-orbital ordering phenomena.[1] One prototypical way to induce these phenomena is the control of the band filling. This may produce the critical state where several electronic phases compete with each other via the modulation of Coulombic correlation, spin and orbital exchange interaction, electron-phonon interaction, and so on. For example, the colossal magnetoresistance is induced by the competition between the ferromagnetic metallic phase and the charge-orbital ordered insulating one.[2,3] Recent extensive studies on colossal magnetoresistance (CMR) in the perovskite-type manganites have revealed that the orbital degrees of freedom play key roles for the versatile magnetic phases and charge transport phenomena. One prominent feature of the CMR manganites related to the orbital degree of freedom is the Jahn–Teller interaction, i.e., the strong coupling of the orbital state with the local lattice distortion to lift the orbital degeneracy. For example, the transition temperature of e_g orbital ordering (OO) in $LaMnO_3$ is as high as 780 K, which is identified as the crystal structure transition. On the contrary, the spin ordering (SO) occurs at a much lower temperature around 140 K.[4] The well separated transition temperatures of OO and SO remain to be observed even in the hole doped system $La_{1-x}Sr_xMnO_3$ until the insulator-metal transition.[5] In other words, the energy scale of the OO coupled with lattice distortion is much larger than that of SO and hence the role of the spin-orbital coupling or the quantum nature of the orbital degree of freedom is not visible in the system.

On the other hand, in the perovskite vanadium oxide RVO_3 (where *R* is a rare earth element), which is known as a prototypical Mott–Hubbard insulator, the t_{2g} orbital is active and the energy scale of the Jahn–Teller interaction is comparable to that of the spin and orbital exchange interaction or the on-site spin-orbit interaction. This enables us to observe the spin-orbital coupled quantum phenomena.[6–9] One prototypical example is the one-dimensional confinement of electrons due to the anisotropic spin-orbital exchange interaction in $LaVO_3$.[6,10] In $LaVO_3$, the two valence electrons occupy the $3d$ t_{2g} orbitals, forming the $S=1$ spin state due to the Hund's-rule coupling. The orthorhombic lattice distortion splits the triply degenerate t_{2g} levels into the lower-lying d_{xy} state and higher-lying doubly degenerate d_{yz} and d_{zx} ones.[11,12] Thus, one electron occupies the d_{xy} orbital and another does either d_{yz} or d_{zx} one. With the decrease in temperature, the *C*-type SO takes place at $T_{SO1}=143$ K and, subsequently, the *G*-type OO does so at $T_{OO1}=141$ K. Here, the *C*-type spin and *G*-type orbital order means that the spins ferromagnetically align along the *c* axis but are alternate in the *ab* plane, while the d_{zx} and d_{yz} orbitals are alternate both along the *c* axis and in the *ab* plane, as schematically shown in Fig. 1.[13–16] In the *C*-type spin and *G*-type orbital ordered phase, the orbital exchange interaction is quasi-one-dimensional due to the interference among the exchange pro-

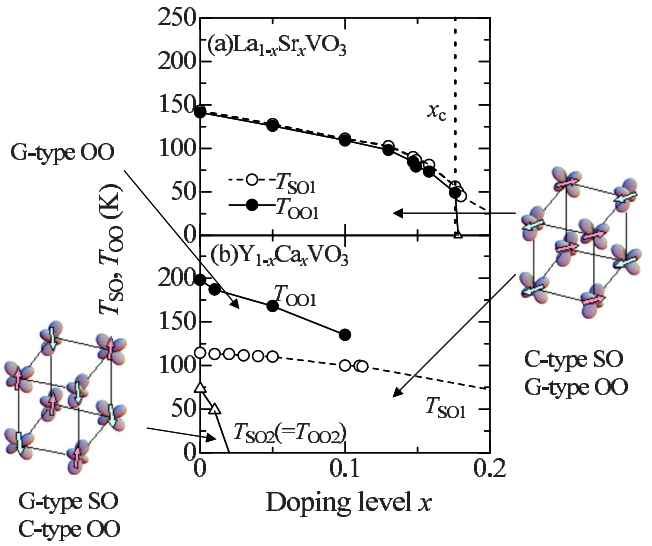

FIG. 1. (Color online) The spin and orbital phase diagram of (a) $La_{1-x}Sr_xVO_3$ and (b) $Y_{1-x}Ca_xVO_3$ plotted against the doping level x as reproduced from Refs. 19 and 25. The closed circles with a solid line, open circles with a dashed line, and open triangles with a solid line indicate the transition temperature of the G-type OO (T_{OO1}), the C-type SO (T_{SO1}), and the G-type SO and C-type OO ($T_{SO2}=T_{OO2}$), respectively. The schematic view shows the patterns of SO and OO. The arrows and lobes indicate spins and d_{zx} or d_{yz} orbitals, respectively. The vertical dotted line in (a) indicates the critical doping level for the insulator-metal transition in $La_{1-x}Sr_xVO_3$, while that for $Y_{1-x}Ca_xVO_3$ positions around $x=0.5$.

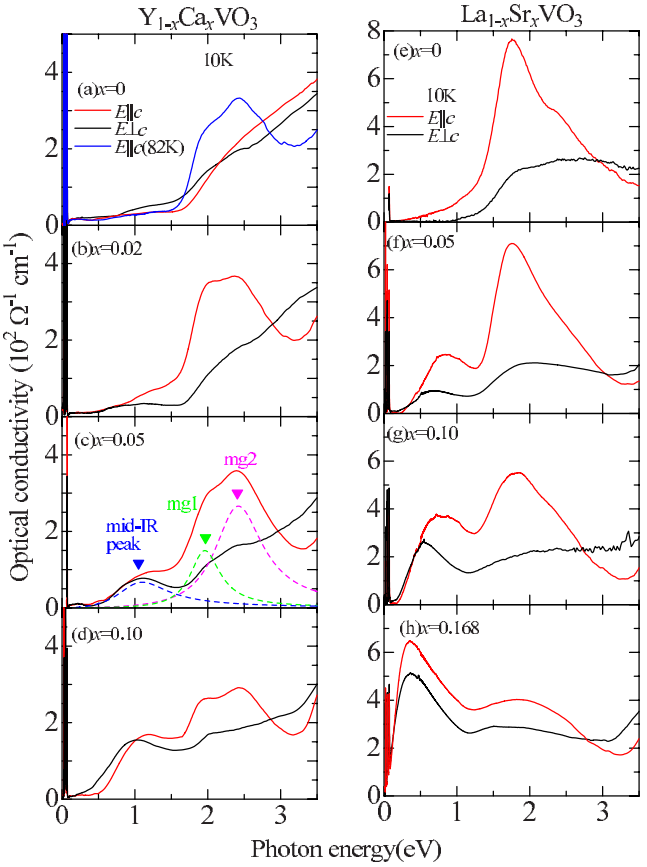

FIG. 2. (Color online) Left panel: Optical conductivity spectra at 10 K for $E\|c$ (red line) and $E\perp c$ (black line) for $Y_{1-x}Ca_xVO_3$ with (a)$x=0$, (b) 0.02, (c) 0.05, and (d) 0.10, respectively. The dashed lines in (c) are the Lorentz oscillators (see text) used for the fitting of the mid-IR peak and two components of the Mott gap excitation, mg1 and mg2, respectively. Right panel: Optical conductivity spectra for $La_{1-x}Sr_xVO_3$ with (e) $x=0$, (f) 0.05, (g) 0.10, and (h) 0.168, respectively.

cesses, leading to the anisotropic feature of the optical Mott-gap excitation.[10,17,18]

By partially replacing the nominally trivalent La ion with the divalent Sr one, i.e., hole doping, the filling-controlled insulator-metal transition is achieved at the critical doping level of $x_c=0.176$.[19,20] The spin-orbital phase diagram in $La_{1-x}Sr_xVO_3$ is shown in Fig. 1(a). With the increase in the doping level x, T_{SO1} and T_{OO1} monotonously decrease and the G-type OO disappears at x_c, while the C-type SO subsists for $x>x_c$. Recently, we have investigated the doping variation of the electronic structure in the course of the insulator-metal transition by measurements of the optical conductivity spectra.[21] We observed that (1) the hole dynamics is anisotropic in the lightly doped region, reflecting the one-dimensional orbital exchange interaction, and (2) the spin and orbital fluctuation is enhanced in the vicinity of the insulator-metal transition, leading to the suppression of the one-dimensional electronic structure.

In another prototypical Mott insulator YVO_3 with a larger $GdFeO_3$-type orthorhombic lattice distortion and hence a smaller one-electron bandwidth, the G-type OO appears at a much higher temperature ($T_{OO1}=200$ K) than the C-type SO ($T_{SO1}=115$ K).[15,22,23] Furthermore, the subsequent spin-orbital phase transition into the G-type spin and C-type orbital ordered phase is observed at $T_{SO2}(=T_{OO2})=77$ K.[24] Recently, we found that this second spin-orbital phase transition is controllable not only by changing temperature but also by the slight variation of the band filling, i.e., hole doping.[25,26] With the increase in x in $Y_{1-x}Ca_xVO_3$, the G-type spin and C-type orbital ordered phase is immediately replaced with the C-type spin and G-type orbital ordered phase at $x=0.02$, as shown in Fig. 1(b). Subsequently, the paramagnetic and G-type orbital ordered phase disappear around $x_o=0.10$. It is anticipated that the Ca substitution arouses the quenched disorder in the lattice sector, which acts as the random potential for the OO and hence destabilizes the OO. This is one possible scenario to explain the fact that the critical doping level for the melting of the G-type OO is smaller in $Y_{1-x}Ca_xVO_3$ ($x_o=0.10$) than in $La_{1-x}Sr_xVO_3$ ($x=x_c=0.176$) since the quenched disorder in the lattice sector originating from the difference in the ionic radii between R and A ions is larger in $Y_{1-x}Ca_xVO_3$ than in $La_{1-x}Sr_xVO_3$. In this paper, we investigate the doping variation of the charge and orbital dynamics in $Y_{1-x}Ca_xVO_3$ by measurements of the polarized optical conductivity and Raman scattering spectra. We discuss the effect of the $GdFeO_3$-type orthorhombic lattice distortion on the evolution of the spin and orbital ordered state with hole doping. The results are argued by comparing with those for $La_{1-x}Sr_xVO_3$ with the larger one-electron bandwidth and the smaller effect of quenched disorder.

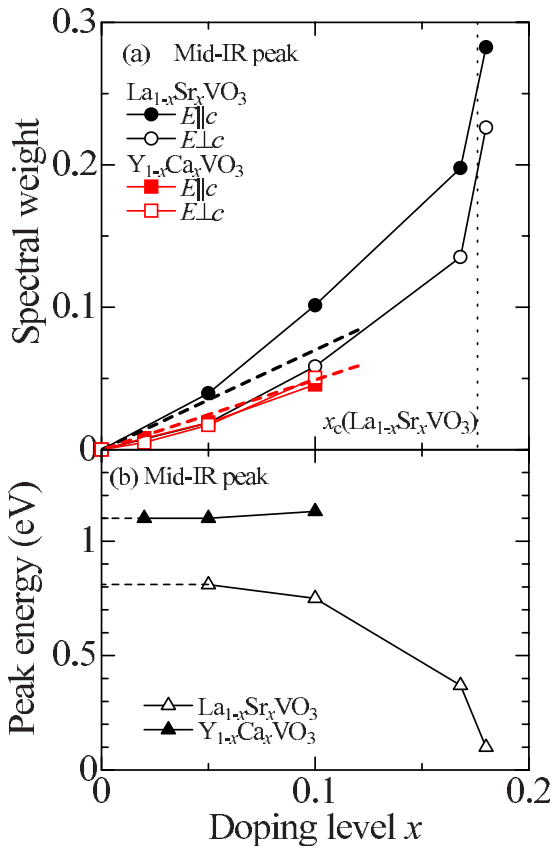

FIG. 3. (Color online) (a) The spectral weight of the mid-IR peak for $E\|c$ (closed squares) and $E\perp c$ (open squares) spectra in $Y_{1-x}Ca_xVO_3$ plotted against x (see text for the definition of the spectral weight). The closed and open circles represent those for $E\|c$ and $E\perp c$ spectra in $La_{1-x}Sr_xVO_3$, respectively. The thick dashed lines are the least-square fitting of the averaged spectral weight $N_{\mathrm{eff}}[\mathrm{av}]=(2N_{\mathrm{eff}}[E\perp c]+N_{\mathrm{eff}}[E\|c])/3$ for $0\le x\le 0.10$ (see text). The vertical dotted line indicates the critical doping level for the insulator-metal transition ($x_c=0.176$) in $La_{1-x}Sr_xVO_3$. (b) The closed and open triangles indicate the energy of the mid-IR peak for $Y_{1-x}Ca_xVO_3$ and $La_{1-x}Sr_xVO_3$ as a function of x, respectively.

The format of this paper is as follows. In Sec. II, we present the experimental procedure. In Sec. III, we present the experimental results and discuss the doping and temperature variation of the charge and orbital dynamics. This section is composed of three parts. In Sec. III A, the optical conductivity spectra at 10 K are presented and the doping variation of the electronic structure of the ground state is discussed. In Sec. III B, the temperature variation of the optical conductivity spectra is presented. We discuss the effect of the $GdFeO_3$-type orthorhombic lattice distortion in the SO and OO. In Sec. III C, we present the Raman scattering spectra and discuss the spin and orbital dynamics in the doped system. The conclusion of this paper is given in Sec. IV.

II. EXPERIMENT

A. Sample preparation

Single crystals of $Y_{1-x}Ca_xVO_3$ were grown by the floating zone method. As starting materials, we used Y_2O_3, $CaCO_3$, and V_2O_5. These powders were mixed and calcined at 600 and 900 °C in flowing Ar/H_2 7% gas. The powders were well ground and calcined again at 1100 °C, and then pressed into a rod, 70 mm long and 5 mm in diameter, which was sintered at 1500 °C in Ar/H_2 7% flowing. The crystal growth was performed with use of a halogen-lamp image furnace at a feed speed of 20 mm/h in flowing Ar gas. We performed a powder x-ray diffraction measurement of the obtained crystal at room temperature and confirmed that the single-phase crystals were obtained.

B. Reflectivity measurements

The temperature dependence of the reflectivity spectra at nearly normal incidence was measured between room temperature and 10 K in the energy region of 0.01–5 eV with linearly polarized light. The crystallographic axes of the samples were determined by a back-Laue method, and the sample surfaces were mechanically polished with alumina powder. In the photon energy region of 0.01–0.7 eV, we used a Fourier transform spectrometer (Bruker-IFS66V). In the region of 0.5–5 eV, we used a grating-type monochromator equipped with a microscope. We carefully mounted samples to ensure the good thermal contact on the thermal conduction type microstat. In the region of 3–40 eV, we carried out the measurement at room temperature (RT) with the use of synchrotron radiation at UV-SOR, Institute for Molecular Science (Okazaki). The RT spectra above 5 eV were connected smoothly with the ones below 5 eV to perform the Kramers–Kronig analysis and obtain the optical conductivity spectra $\sigma(\omega)$ at respective temperatures. For the analysis, we assumed a constant reflectivity below 0.01 eV and also used ω^{-4} extrapolation above 40 eV.

C. Raman scattering measurements

The Raman spectra were measured using a temperature-variable cryostat and the triple-grating spectrometer equipped with a microscope and liquid-nitrogen-cooled charge coupled device detector. The sample surfaces were mechanically polished with alumina powder and annealed at 1000 °C in Ar/H_2 7% gas flow. The 2.410 eV (514.5 nm) line from an Ar ion laser was utilized for the excitation. The spot size of the laser for the excitation was about 4 μm, while the power was reduced to 0.3 mW to avoid the heating effect. We collected the scattered light in backscattering geometry. The polarized geometry is described using the conventional notation $k_i(e_ie_s)k_s$, where k_i and e_i represent the propagation direction and the polarization of the incident light, respectively, and k_s and e_s represent those of the scattering light. The spectra were measured with the polarization configuration $y(xx)\bar{y}$, where x and y are the (110) and $(1\bar{1}0)$ crystal direction in the orthorhombic ($Pbnm$) setting. All the spectra were calibrated by the instrumental sensitivity.

III. RESULTS AND DISCUSSION

A. Doping variation of the electronic structure in the ground state

In this section, we discuss the doping variation of the optical conductivity spectra at the ground state. The ground

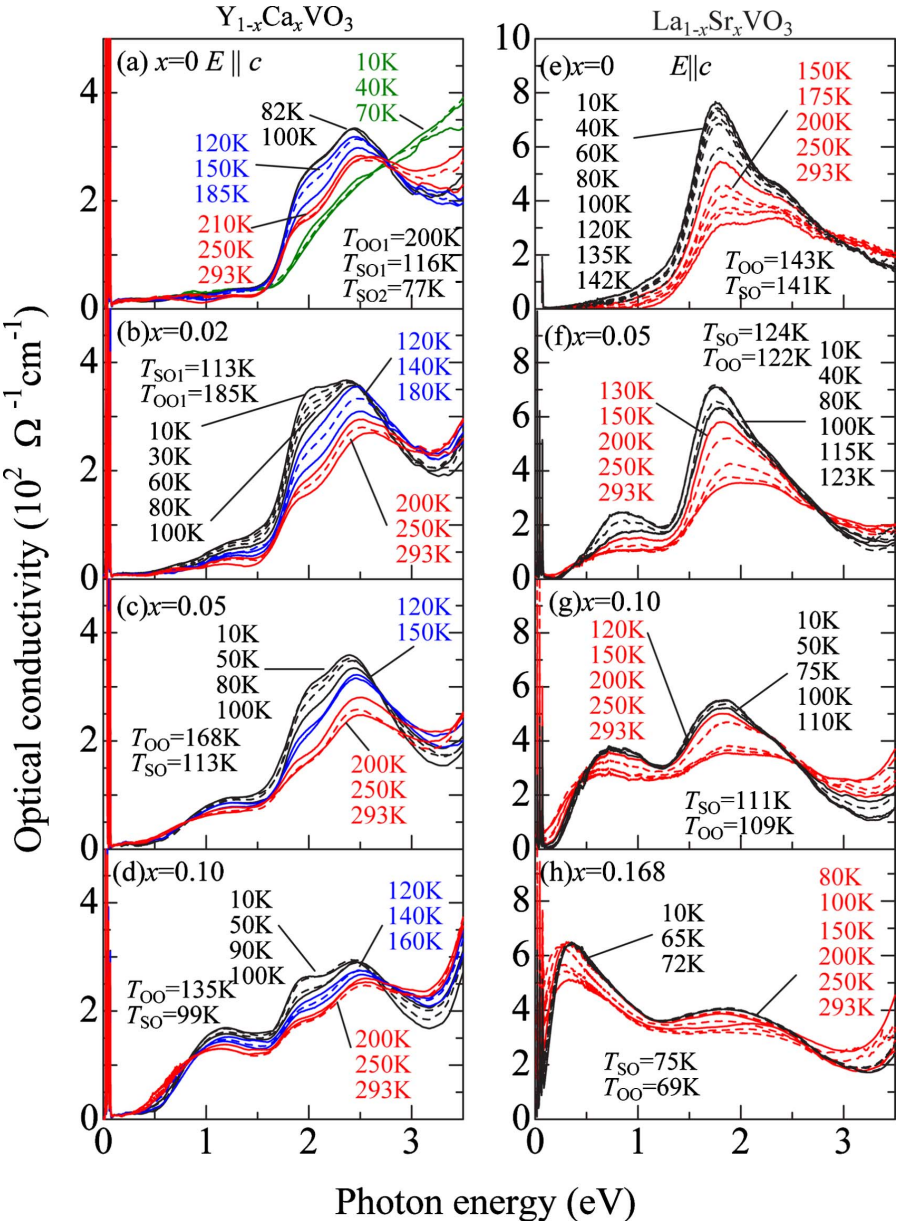

FIG. 4. (Color online) Left panel: The temperature dependence of the optical conductivity spectra for $Y_{1-x}Ca_xVO_3$ with (a) $x=0$, (b) 0.02, (c) 0.05, and (d) 0.10, respectively. Right panel: The temperature dependence of the optical conductivity spectra for $E\|c$ in $La_{1-x}Sr_xVO_3$ with (e) $x=0$, (f) 0.05, (g) 0.10, and (h) 0.168, respectively.

state of $Y_{1-x}Ca_xVO_3$ changes from the G-type spin and C-type orbital ordered phase to the C-type spin and G-type orbital ordered one with hole doping beyond $x=0.02$. In Fig. 2, we show the polarization dependence of the optical conductivity spectra of $Y_{1-x}Ca_xVO_3$ with $x=0$, 0.02, 0.05, and 0.10 at 10 K and reproduce those of $La_{1-x}Sr_xVO_3$ with $x=0$, 0.05, 0.10, and 0.168 for comparison.[21] For $x=0$ in $Y_{1-x}Ca_xVO_3$, both the $E\|c$ and $E\perp c$ spectra show the clear onset of the conductivity at around 1.5 eV, which is assigned to the Mott gap excitation in the $3d\ t_{2g}$ band of V ions,[18,20,27] and the shape of the spectra is nearly isotropic. This behavior is contrasted with the spectral shape for $x=0.02$, where the SO and OO are C-type and G-type, respectively. For $x=0.02$, the spectra show a clear peak structure of the Mott-gap excitation around 2.5 eV for $E\|c$, while those for $E\perp c$ appear to be nearly identical to those for $x=0$. Such an anisotropic feature is similarly observed in the spectra of $LaVO_3$ at 10 K and YVO_3 at $T>T_{SO2}$. The recent theoretical calculation has shown that the Mott-gap excitation strongly depends on the spin and orbital exchange interaction and that the anisotropic Mott-gap excitation in the C-type spin and G-type orbital ordered phase originates from the one-dimensional orbital exchange interaction.[10,17] In other words, the nearly isotropic spectra of YVO_3 ($x=0$) at 10 K imply that the orbital exchange interaction in the G-type spin ordered state is nearly isotropic in magnitude. The present result for YVO_3 is not consistent with that of the previous paper by Miyasaka *et al.*,[28] but rather in accord with that of the ellipsometry measurement by Tsvetkov *et al.*[29] They reported that the anisotropic feature of the Mott-gap excitation

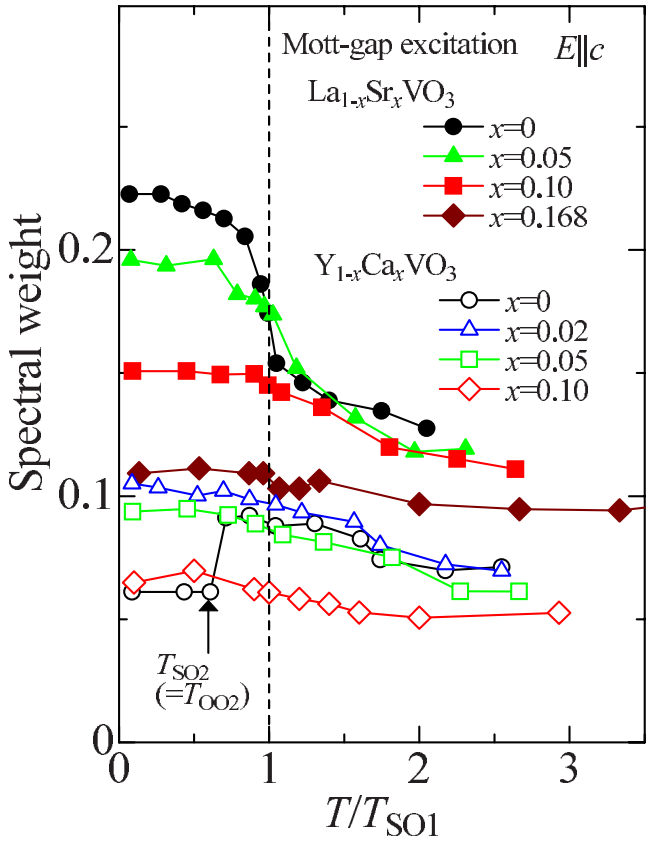

FIG. 5. (Color online) (a) The spectral weight of the Mott-gap excitation N_{eff}^{mg} for $E\|c$ spectra in $La_{1-x}Sr_xVO_3$ with $x=0$, 0.05, 0.10, and 0.168 (closed circles, triangles, squares, and diamonds, respectively) and in $Y_{1-x}Ca_xVO_3$ with $x=0$, 0.02, 0.05, and 0.10 (open circles, triangles, squares, and diamonds, respectively) plotted against the normalized temperature T/T_{SO1}.

is reduced in the G-type spin and C-type orbital ordered phase.

For $x=0.05$, in addition to the reminiscence of the Mott-gap excitation around 2.5 eV, a new peak structure shows up around 1 eV. A similar peak structure is observed in $La_{1-x}Sr_xVO_3$ with $x=0.05$, 0.10, and 0.168, as shown in Figs. 2(f)–2(h), and attributed to the dynamics of the doped hole. It is anticipated from the highly insulating charge transport that the doped hole is trapped to form the small polaronlike state accompanying the lattice relaxation with the modification in the spin and orbital sectors.[20,21] In this paper, we call the new peak "mid-IR peak" in the following. Although the reminiscence of the Mott-gap excitation clearly shows an anisotropic feature, the mid-IR peak appears nearly isotropic. This is contrasted to the case of $La_{1-x}Sr_xVO_3$, where the mid-IR peak also shows anisotropy as well as the Mott-gap excitation in such a lightly doped region as $x=0.05$. For $Y_{1-x}Ca_xVO_3$ with $x=0.10$, where the high-temperature G-type orbital ordered phase barely subsists, the reminiscence of the Mott-gap excitation still shows anisotropy and the intensity of the mid-IR peak becomes larger than that for $x=0.05$.

To estimate the spectral weight of the mid-IR peak more quantitatively, we fitted spectra with the Lorentz-type oscillators,

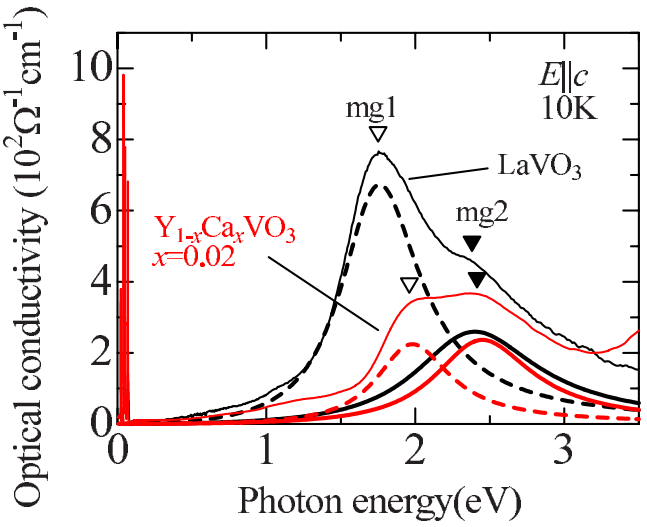

FIG. 6. (Color online) Optical conductivity spectra at 10 K for $E\|c$ in $Y_{1-x}Ca_xVO_3$ with $x=0.02$ and $LaVO_3$, respectively. The thick dashed and solid lines represent the Lorentz oscillators assumed for the fitting of the two components of the Mott-gap excitation, mg1 and mg2, respectively.

$$\sigma(\omega) = \sum_{j=m,\mathrm{mg1},\mathrm{mg2},ct} \frac{S_j \gamma_j \omega^2 \omega_j^2}{(\omega^2 - \omega_j^2)^2 + \gamma_j^2 \omega^2},$$

and calculated the spectral weight, namely, the effective number of electrons $N_{\mathrm{eff}}(=2m/\pi e^2 N \int_0^\infty \sigma(\omega)d\omega)$. Here, m, mg1, mg2, and ct represent the component of the mid-IR peak, the two components of Mott-gap excitation, and the charge-transfer excitation from O $2p$ to V $3d$ band, respectively. As assigned in the previous work,[18] the lower-lying mg1 band is an allowed Mott-gap transition along the ferromagnetic chain ($\|c$) in the C-type spin ordered phase, while the higher-lying mg2 band would be nominally forbidden in the case of the perfect spin and orbital polarization in the cubic perovskite lattice. The latter turns to be visible possibly due to the imperfect spin and orbital polarization and/or to the orthorhombic lattice distortion. In Fig. 3(a), we show the doping variation of N_{eff} of the mid-IR peak (N_{eff}^m) for $E\|c$ and $E\perp c$ in $Y_{1-x}Ca_xVO_3$ as well as that in $La_{1-x}Sr_xVO_3$. The N_{eff}^m values for $E\|c$ and $E\perp c$ monotonously increase with the increase in x. It should be noted again that N_{eff}^m for $E\|c$ is comparable to that for $E\perp c$ in $Y_{1-x}Ca_xVO_3$ with $x\leq 0.1$, in spite of the anisotropic Mott-gap excitation. This is contrasted to the case of $La_{1-x}Sr_xVO_3$, where N_{eff}^m in the lightly doped region (e.g., $x=0.05$) is larger for $E\|c$ than for $E\perp c$ as well as that of Mott-gap excitation. To see the variation of the kinetic energy of the doped hole, we calculated the averaged spectral weight $N_{\mathrm{eff}}[\mathrm{av}]=(2N_{\mathrm{eff}}[E\perp c]+N_{\mathrm{eff}}[E\|c])/3$ at various x (data are not shown to avoid complexity in the figure) and performed least-square fitting for $x\leq 0.1$, the results of which are shown with thick dashed lines in Fig. 3(a). The gradient of the least-square fitted line for $Y_{1-x}Ca_xVO_3$ is around 2/3 of that for $La_{1-x}Sr_xVO_3$, indicating the smaller kinetic energy of the doped hole in $Y_{1-x}Ca_xVO_3$ than in $La_{1-x}Sr_xVO_3$. This is explained in terms of the variation of the effective electron correlation U/W (where U and W rep-

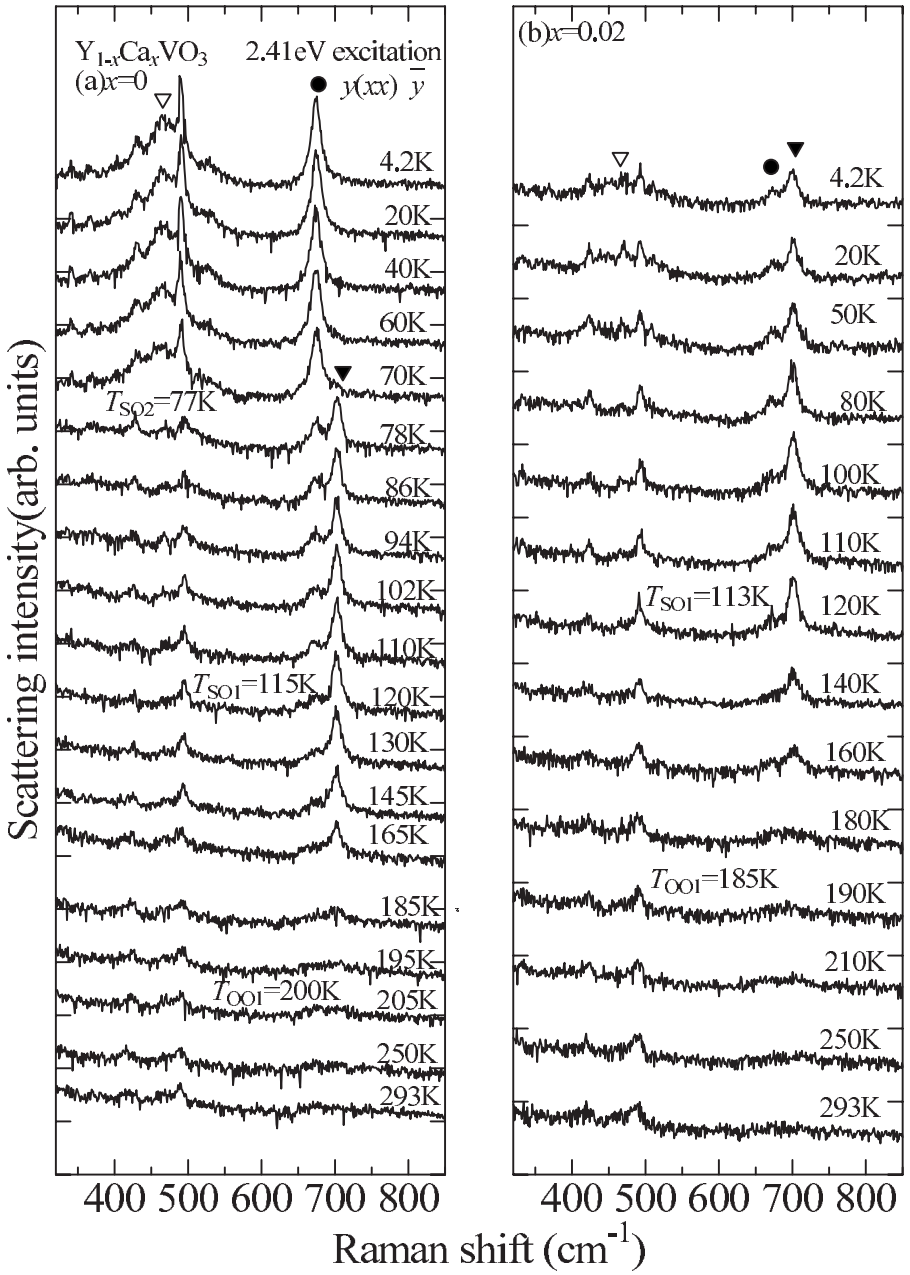

FIG. 7. Raman scattering spectra for the polarization configuration of $y(xx)\bar{y}$ at various temperatures in $Y_{1-x}Ca_xVO_3$ with (a) $x=0$ and (b) $x=0.02$, measured with the excitation photon energy of 2.410 eV. The broadband around 470 cm^{-1} (open triangle), peak structure around 670 cm^{-1} (closed circle), and that around 700 cm^{-1} (closed triangle) are assigned to the two-magnon band, the oxygen stretching mode coupled with the *C*-type OO and that coupled with the *G*-type OO, respectively.

resent the Coulombic correlation energy and the one-electron bandwidth, respectively). The larger $GdFeO_3$-type orthorhombic lattice distortion in $Y_{1-x}Ca_xVO_3$ than that in $La_{1-x}Sr_xVO_3$ results in the smaller V–O–V bond angle, leading to the larger effective U/W for the V $3d\ t_{2g}$ band, or the suppression of the hole kinetic energy. A similar relation of the kinetic energy of the doped hole with the effective U/W has also been examined for the filling-controlled perovskite titanates $R_{1-x}A_xTiO_3$.[30] In general, the electron-lattice coupling plays a cooperative role in localizing the charged carrier with the electron correlation. By means of the dynamical mean-field theory, Millis *et al.*[31] pointed out that the lattice relaxation around the localized electron increases with the reduction in the kinetic energy via the dimensionless parameter $\lambda=g^2/kt$ (here, g is the coupling constant of electron-phonon interaction, k is the elastic energy of the lattice, and t is the transfer energy of electron). In the present system, it is expected that the increase in U/W enhances the local lattice relaxation accompanying the local modification in the spin and orbital sectors around the doped hole. Since the dynamics of the doped hole is sensitive to the spin and orbital states on the neighboring sites, this could explain the less anisotropic hole dynamics in $Y_{1-x}Ca_xVO_3$ than in $La_{1-x}Sr_xVO_3$. In addition, the enhanced modification in the

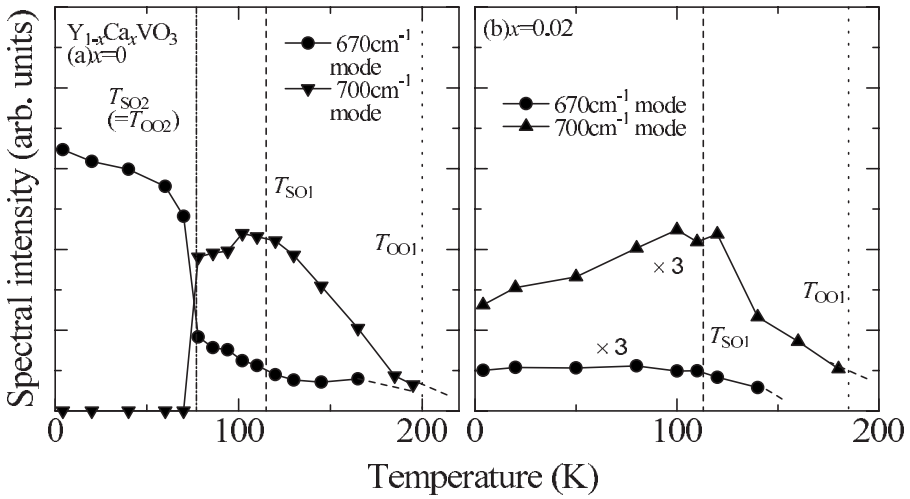

FIG. 8. Temperature dependence of the spectral intensity of the phonon peaks around 670 cm^{-1} (closed circle) and 700 cm^{-1} (closed triangle) in $Y_{1-x}Ca_xVO_3$ with (a) $x=0$ and (b) $x=0.02$, respectively. The dash-dotted, dashed, and dotted lines indicate $T_{SO2}(=T_{OO2})$, T_{SO1}, and T_{OO1}, respectively.

spin and orbital sectors tends to destabilize the long-range SO and OO. Thus, as well as the quenched disorder in the lattice sector, which is argued in Sec. I, this may also explain why the critical doping level required for the melting of the G-type OO is lower in $Y_{1-x}Ca_xVO_3$ ($x_o=0.10$) than in $La_{1-x}Sr_xVO_3$ ($x=x_c=0.176$).

In Fig. 3(b), we plot the x variation of the mid-IR peak energy for $E\|c$ spectra ($\omega_{m\|}$) in $Y_{1-x}Ca_xVO_3$ compared to that in $La_{1-x}Sr_xVO_3$ as a measure of the excitation energy of the doped hole from the self-trapped state. In both $Y_{1-x}Ca_xVO_3$ and $La_{1-x}Sr_xVO_3$, the $\omega_{m\|}$ is nearly constant for $x\leq 0.1$, indicating that the doped holes are well localized and the interaction among them is negligible. In the dilute limit ($x\rightarrow 0$), the $\omega_{m\|}$ in $Y_{1-x}Ca_xVO_3$ seems to be larger than that in $La_{1-x}Sr_xVO_3$. This is in accord with the anticipation that the larger lattice relaxation accompanying the larger modification in the spin and orbital sectors would trap doped holes at a deeper energy-level state.

B. Temperature variation of the optical conductivity spectra for $Y_{1-x}Ca_xVO_3$

In this section, we present the temperature variation of the optical conductivity spectra for $Y_{1-x}Ca_xVO_3$ in comparison to the case for $La_{1-x}Sr_xVO_3$ and discuss the effect of the $GdFeO_3$-type orthorhombic lattice distortion on the spin and orbital ordered states. Since the optical conductivity spectra for $E\perp c$ show minimal temperature variation, we focus on those for $E\|c$ in the following discussion. Figures 4(a)–4(d) show the temperature variation of the optical conductivity spectra for $E\|c$ in $Y_{1-x}Ca_xVO_3$, with $x=0$, 0.02, 0.05, and 0.10, respectively. For $x=0$, the spectra show minimal temperature variation within the G-type spin and C-type orbital ordered phase, i.e., at $T<T_{SO2}(=T_{OO2})$. At $T>T_{SO2}$, as mentioned in Sec. III A, the spectra show a clear peak structure around 2.5 eV, which reflects the one-dimensional orbital exchange interaction and decreases in its magnitude with the increase of temperature. Such a conspicuous suppression of the intensity of the Mott-gap excitation with the increase in temperature is similar to the case for $LaVO_3$, as shown in Fig. 4(e), and is attributed to the crossover from the one-dimensional to three-dimensional exchange interaction in the orbital sector.[10,17,18] In the doped systems, such as $x=0.02$, 0.05, and 0.10, the intensity of the Mott-gap excitation monotonously decreases with the increase in temperature and the magnitude of the temperature variation also decreases with the increase in x. A similar behavior is observed in $La_{1-x}Sr_xVO_3$ and attributed to the reduction of the spin and orbital correlation.[21]

To estimate the temperature variation of the spectral weight of the Mott-gap excitation more quantitatively, we calculated N_{eff} of the Mott-gap excitation (N_{eff}^{mg}) by using the fitting formula described in the Sec. III A. In Fig. 5, we plot the values for $Y_{1-x}Ca_xVO_3$ and $La_{1-x}Sr_xVO_3$ at various x as a function of the normalized temperature (T/T_{SO1}). Here, N_{eff}^{mg} is defined as the sum of the two components of the Mott-gap excitation, i.e., mg1 and mg2. For $LaVO_3$ ($x=0$), N_{eff}^{mg} steeply decreases around T_{SO1} with the increase in temperature. This behavior is consistent with the recent x-ray diffraction study by Ren *et al.*[16] They reported that the phase transition to the G-type OO at T_{OO1} in $LaVO_3$ is of the first order. With the increase in x in $La_{1-x}Sr_xVO_3$, the steep change of N_{eff}^{mg} around T_{SO1} is extinguished, although the temperature variation is still visible at $x=0.168$, i.e., on the verge of the insulator-metal transition accompanying the orbital order-disorder transition.

In $Y_{1-x}Ca_xVO_3$, the temperature variation of N_{eff}^{mg} is different from that in $La_{1-x}Sr_xVO_3$. For $x=0$, N_{eff}^{mg} shows a clear jump at T_{SO2}, reflecting the onset of the one-dimensional orbital exchange interaction inherent in the C-type spin and G-type orbital ordered phase. At $T>T_{SO2}$, with the increase in temperature, N_{eff}^{mg} monotonously decreases down to the room temperature as well as that in $La_{1-x}Sr_xVO_3$. In the doped systems $Y_{1-x}Ca_xVO_3$ with $x=0.02$, 0.05, and 0.10, a similar behavior is observed, apart from the absence of the G-type spin and C-type orbital ordered phase as the ground state. It should be noted that N_{eff}^{mg} is less temperature-

dependent for $Y_{1-x}Ca_xVO_3$ than for $La_{1-x}Sr_xVO_3$, at the respective doping levels x. This suggests that the increasing $GdFeO_3$-type orthorhombic lattice distortion tends to reduce the one dimensionality of the orbital exchange interaction. To see the influence of the $GdFeO_3$-type orthorhombic lattice distortion more explicitly, we show the optical conductivity spectra for $Y_{1-x}Ca_xVO_3$ with $x=0.02$ and $LaVO_3$ at 10 K in Fig. 6. Since $N_{\mathrm{eff}}^{\mathrm{mg}}$ for $x=0.02$ is nearly identical to that for $x=0$ at $T>T_{SO2}$, the reduction of the spin and orbital correlation by the doped hole is negligible at such a low doping level. Although it is difficult to accurately distinguish the spectral weight of mg1 from that of mg2, the former appears to be much smaller in $Y_{1-x}Ca_xVO_3$ with $x=0.02$ than in $La_{1-x}Sr_xVO_3$ ($x=0$ or 0.05), while the latter appears to be nearly comparable.

On the basis of these results, we discuss the lattice effect on the electronic structure. The present observation suggests that the $GdFeO_3$-type orthorhombic lattice distortion selectively suppresses the lower-lying allowed band (mg1) relatively to the higher-lying (nominally forbidden) one (mg2). The plausible explanation may be given by the deviation of the SO and OO from the pure C type and G type, respectively. Recently, DeRaychaudhury *et al.*[32] performed the *ab initio* calculation combined with the dynamical mean-field theory and pointed out that the variation of the crystal field at V sites due to the $GdFeO_3$-type orthorhombic lattice distortion plays an important role for the OO as well as the Jahn–Teller effect. They showed that the $GdFeO_3$-type orthorhombic lattice distortion tends to stabilize the C-type OO and induces the C-type character of the OO even in the G-type OO via the cation covalency between R and V ions. The spin and lattice dynamics coupled with such a modified OO is the issue to be discussed in Sec. III C.

C. Dynamic spin-orbital phase fluctuation

In this section, we discuss the doping variation of the spin excitation and lattice dynamics coupled with the OO in $Y_{1-x}Ca_xVO_3$. As for the undoped systems, we recently investigated spin and orbital dynamics by measurements of the temperature variation of the Raman scattering spectra.[33] As the starting point of the following discussion, we first reproduce in Fig. 7(a) the temperature variation of the Raman scattering spectra for YVO_3 with the polarization configuration of $y(xx)\bar{y}$, which was obtained by utilizing the Ar ion laser 2.410 eV (514.5 nm) line as an excitation light. The polarized geometry is as described in Sec. II C. In the G-type spin and C-type orbital ordered phase ($T<T_{SO2}$), the broad two-magnon band and the oxygen stretching mode coupled with the C-type OO are observed around 470 cm^{-1} and 670 cm^{-1}, respectively. At $T>T_{SO2}$, the oxygen stretching mode coupled with the G-type OO appears around 700 cm^{-1}, but that coupled with the C-type OO remains to be observed. Similarly, the broad two-magnon band is still discerned, although its intensity is severely reduced. In Fig. 8(a), the temperature variation of the spectral intensity of each mode is reproduced. With the increase in temperature, the spectral intensity of the 670 cm^{-1} mode coupled with the C-type OO decreases discontinuously at T_{SO2} but still remains finite at $T>T_{SO2}$. On the other hand, the spectral intensity of the 700 cm^{-1} mode coupled with the G-type OO abruptly emerges above $T_{SO2}=(T_{OO2})$, reaches maximum around 100 K, and finally monotonously decreases with the increase in temperature. These results are interpreted as the subsistence of the G-type spin and C-type orbital component in the nominally C-type spin and G-type orbital ordered phase.[9,33] In Fig. 7(b), we comparatively show the temperature variation of the Raman scattering spectra for $x=0.02$ with the polarization configuration of $y(xx)\bar{y}$ measured in the same condition. Although the ground state of this system is turned to the nominally C-type spin and G-type orbital ordered phase, the broad two-magnon band characteristic of the G-type SO and the oxygen stretching mode coupled with the C-type OO are observed around 470 and 670 cm^{-1} at low temperatures, respectively, as in the case of YVO_3. We also plot the temperature variation of the spectral intensity of the two (670 and 700 cm^{-1}) oxygen stretching modes for $x=0.02$ in Fig. 8(b). With increasing temperature, the spectral intensity of the 700 cm^{-1} mode monotonously increases up

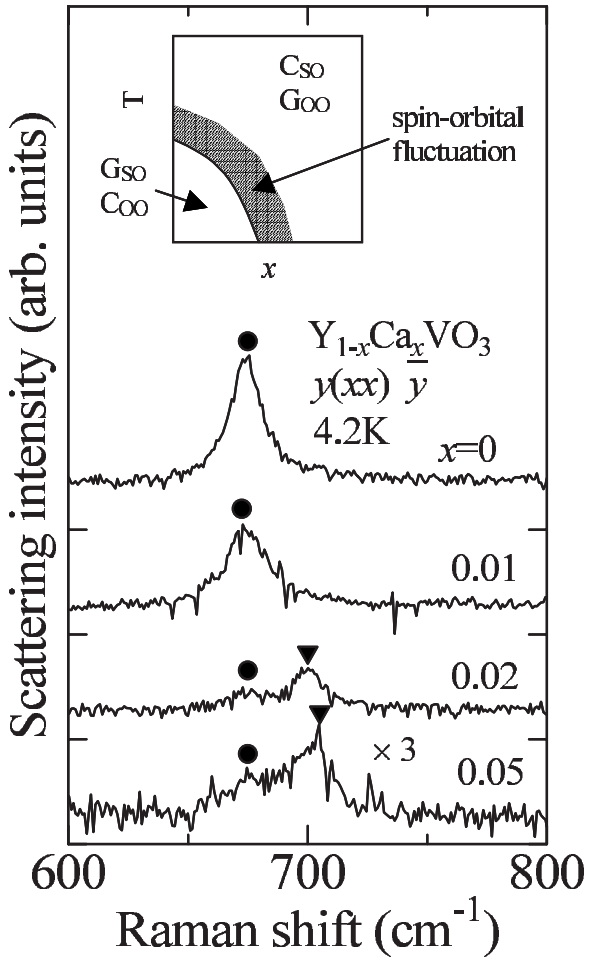

FIG. 9. Raman scattering spectra at 4.2 K in $Y_{1-x}Ca_xVO_3$ with various x, measured with the excitation photon energy of 2.410 eV. The closed circles and triangles indicate the 670 and 700 cm^{-1} oxygen stretching mode, respectively. The inset is the pictorial view of the spin-orbital phase diagram in x-T plane in a low temperature region. The hatched region indicates the phase where the dynamical G-type spin and C-type orbital correlation exists.

to around T_{SO1} and decreases at $T > T_{SO1}$, while the 670 cm^{-1} mode monotonously decreases above T_{SO1}.

One possible scenario to explain the double peak structure of the oxygen stretching mode and the subsistence of the broad two-magnon band would be the static phase separation into the two competing phases; the phase separation is generally observed in the phase competing systems subject to quenched disorder.[34] A recent neutron experiment, however, has revealed that the magnetic structure of the $Y_{1-x}Ca_xVO_3$ ($x=0.02$) crystal coming from the same batch is nearly uniform *C*-type at low temperatures.[35] This excludes the above mentioned phase separation model. Thus, a more plausible explanation is the existence of the dynamical *G*-type spin and *C*-type orbital correlation. This scenario is consistent with both the results of neutron diffraction and Raman scattering, since the (elastic) diffraction probe can hardly capture the rapid dynamical spin fluctuation. It should be noted that our result is contrasted with the recent x-ray diffraction experiment on $SmVO_3$, in which the static phase separation between the two competing phases is observed down to low temperatures.[36] In the present system, however, the microscopic phase separation is not favored perhaps due to the energy cost at the interface of two competing phases, although the inhomogeneity is induced by the well localized doped-hole. The unit cell volume in the *G*-type spin and *C*-type orbital ordered phase is different as much as by 0.16% from that in the *C*-type spin and *G*-type orbital ordered one.[22] Therefore, the lattice strain at the interface between the two phases would cost too much energy to establish the phase-separated state in the single-domain single crystal.

The *G*-type spin and *C*-type orbital correlation in the present case survives even away from the phase boundary. In Fig. 9, we show the doping variation of the Raman scattering spectra with the polarization configuration of $y(xx)\bar{y}$ at 10 K. With the increase in x, the spectral intensity of the 670 cm^{-1} mode monotonously decreases, reflecting the reduction in the correlation of the *C*-type OO, but keeps a finite intensity even at $x=0.05$ as well as the 700 cm^{-1} one. Thus, it is expected that the dynamical *G*-type spin and *C*-type orbital correlation remains up to a high-doped region at low temperatures, as schematically shown in the inset of Fig. 9. This is contrasted to the case for $La_{1-x}Sr_xVO_3$, in which the ground state remains to be the pure *C*-type spin and *G*-type orbital ordered states up to the insulator-metal transition point ($x_c=0.176$).

IV. CONCLUSION

In conclusion, we have investigated the spin and orbital states in $Y_{1-x}Ca_xVO_3$ by measurements of the optical conductivity and Raman scattering spectra with focus on the hole doping effect on the two competing spin and orbital ordered phases. We compared the results to those for another canonical system $La_{1-x}Sr_xVO_3$, which shows less orthorhombic lattice distortion and larger one-electron bandwidth. The doped hole forms the self-trapped small polaronlike state with the lattice relaxation accompanying the modification in the spin and orbital sectors. The distortion in the spin, orbital, and lattice sectors appears to be enhanced by the decrease in the one-electron bandwidth, i.e., in going from $La_{1-x}Sr_xVO_3$ to $Y_{1-x}Ca_xVO_3$. This explains the observed feature that the hole dynamics in $Y_{1-x}Ca_xVO_3$ is less sensitive to the evolution of the spin and orbital ordering and is nearly isotropic even in the lightly doped region. This is contrasted to the anisotropic hole dynamics observed in the lightly doped region of $La_{1-x}Sr_xVO_3$. The modest temperature variation and small spectral weight of the lower-lying allowed Mott-gap excitation suggests that the OO deviates from the pure *G*-type. At low temperatures, the broad two-magnon band and the oxygen stretching mode inherent in the *G*-type spin and *C*-type orbital ordered phase are persistently observed in the Raman scattering spectra for the doping induced phase ($x \geq 0.02$) of the nominally *C*-type SO and *G*-type OO, indicating the subsistence of the dynamical *G*-type spin and *C*-type orbital correlation.

ACKNOWLEDGMENTS

We thank B. Keimer, C. Ulrich, and M. Reehuis for discussion. One of the authors (J.F.) was supported by the Japan Society for the Promotion of Science for Young Scientists. This work was supported in part by the Grant-In-Aid for Scientific Research (Grants No. 15104006, No. 17340104, and No. 16076205) from MEXT of Japan.

[1] For a review, see M. Imada, A. Fujimori, and Y. Tokura, Rev. Mod. Phys. **70**, 1039 (1998).
[2] Y. Tokura and N. Nagaosa, Science **288**, 462 (2000).
[3] For a review, see, for example, Y. Tokura, Rep. Prog. Phys. **69**, 797 (2006).
[4] Y. Murakami, J. P. Hill, D. Gibbs, M. Blume, I. Koyama, M. Tanaka, H. Kawata, T. Arima, Y. Tokura, K. Hirota, and Y. Endoh, Phys. Rev. Lett. **81**, 582 (1998).
[5] V. A. Ivanshin, J. Deisenhofer, H. A. Krug von Nidda, A. Loidl, A. A. Mukhin, A. M. Balbashov, and M. V. Eremin, Phys. Rev. B **61**, 6213 (2000).
[6] G. Khaliullin, P. Horsch, and A. M. Oles, Phys. Rev. Lett. **86**, 3879 (2001).
[7] J. Sirker and G. Khaliullin, Phys. Rev. B **67**, 100408(R) (2003).
[8] P. Horsch, G. Khaliullin, and A. M. Oles, Phys. Rev. Lett. **91**, 257203 (2003).
[9] C. Ulrich, G. Khaliullin, J. Sirker, M. Reehuis, M. Ohl, S. Miyasaka, Y. Tokura, and B. Keimer, Phys. Rev. Lett. **91**, 257202 (2003).
[10] Y. Motome, H. Seo, Z. Fang, and N. Nagaosa, Phys. Rev. Lett. **90**, 146602 (2003).
[11] T. Mizokawa and A. Fujimori, Phys. Rev. B **54**, 5368 (1996).
[12] H. Sawada, N. Hamada, K. Terakura, and T. Asada, Phys. Rev. B **53**, 12742 (1996).

[13] V. G. Zubkov, G. V. Bazuev, and G. P. Shveikin, Sov. Phys. Solid State **18**, 1165 (1976).
[14] P. Bordet, C. Chaillout, M. Maezono, Q. Huang, A. Santoro, S-W. Cheong, H. Takagi, C. S. Oglesby, and B. Batlogg, J. Solid State Chem. **106**, 253 (1993).
[15] S. Miyasaka, Y. Okimoto, M. Iwama, and Y. Tokura, Phys. Rev. B **68**, 100406(R) (2003).
[16] Y. Ren, A. A. Nugroho, A. A. Menovsky, J. Strempfer, U. Rutt, F. Iga, T. Takabatake, and C. W. Kimball, Phys. Rev. B **67**, 014107(2003).
[17] G. Khaliullin, P. Horsch, and A. M. Oles, Phys. Rev. B **70**, 195103 (2004).
[18] S. Miyasaka, Y. Okimoto, and Y. Tokura, J. Phys. Soc. Jpn. **71**, 2086 (2002).
[19] S. Miyasaka, T. Okuda, and Y. Tokura, Phys. Rev. Lett. **85**, 5388 (2000).
[20] F. Inaba, T. Arima, T. Ishikawa, T. Katsufuji, and Y. Tokura, Phys. Rev. B **52**, R2221 (1995).
[21] J. Fujioka, S. Miyasaka, and Y. Tokura, Phys. Rev. Lett. **97**, 196401 (2006).
[22] G. R. Blake, T. T. M. Palstra, Y. Ren, A. A. Nugroho, and A. A. Menovsky, Phys. Rev. B **65**, 174112 (2002).
[23] M. Noguchi, A. Nakazawa, S. Oka, T. Arima, Y. Wakabayashi, H. Nakao, and Y. Murakami, Phys. Rev. B **62**, R9271 (2000).
[24] H. Kawano, H. Yoshizawa, and Y. Ueda, J. Phys. Soc. Jpn. **63**, 2857 (1994).
[25] J. Fujioka, S. Miyasaka, and Y. Tokura, Phys. Rev. B **72**, 024460 (2005).
[26] S. Ishihara, Phys. Rev. Lett. **94**, 156408 (2005).
[27] Z. Fang, N. Nagaosa, and K. Terakura, Phys. Rev. B **67**, 035101 (2003).
[28] In the previous paper (Ref. 18), the optical conductivity spectra of YVO_3 show the anisotropic Mott-gap excitation even at $T < T_{SO2}$. This discrepancy perhaps results from the wrong setting of the sample temperature in the previous work. A crystal of YVO_3 tends to be cracked during the measurements in warming or cooling process especially around $T=T_{SO2}$, which degrades the thermal conduction between the sample surfaces and the cold finger of the cryostat. Thus, we carefully mounted samples and checked the reproducibility of the data by measuring the spectra several times both in the warming and in cooling processes. It is likely that the sample surface was not cooled down enough below T_{SO2} in the previous work of Ref. 18.
[29] A. A. Tsvetkov, F. P. Mena, P. H. M. vanLoosdrecht, D. vander-Marel, Y. Ren, A. A. Nugroho, A. A. Menovsky, I. S. Elfimov, and G. A. Sawatzky, Phys. Rev. B **69**, 075110 (2004).
[30] T. Katsufuji, Y. Okimoto, and Y. Tokura, Phys. Rev. Lett. **75**, 3497 (1995).
[31] A. J. Millis, R. Mueller, and B. I. Shraiman, Phys. Rev. B **54**, 5389 (1996).
[32] M. DeRaychaudhury, E. Pavarini, and O. K. Andersen, Phys. Rev. Lett. **99**, 126402 (2007).
[33] S. Miyasaka, J. Fujioka, M. Iwama, Y. Okimoto, and Y. Tokura, Phys. Rev. B **73**, 224436 (2006).
[34] E. Dagotto, Science **309**, 257 (2005).
[35] M. Reehuis *et al.* (unpublished).
[36] M. H. Sage, G. R. Blake, G. J. Nieuwenhuys, and T. T. M. Palstra, Phys. Rev. Lett. **96**, 036401 (2006).